Phase Separation Mechanism During Membrane Formation by Dry-Cast Process

HIDETO MATSUYAMA, MANABU NISHIGUCHI, YOSHIRO KITAMURA

Department of Environmental Chemistry and Materials, Okayama University, 2-1-1 Tsushima-naka, Okayama 700-8530, Japan

Received 12 March 1999; accepted 16 October 1999

ABSTRACT: Phase separation mechanisms during the membrane formation by dry-cast process were investigated by light scattering in the cellulose acetate/dimethylformamide (DMF)/2-methyl-2,4-pentanediol system. Phase separation occurred by spinodal decomposition (SD) when paths of the composition changes due to the evaporation of DMF were close to the critical point in the phase diagram. Characteristic properties of the early stage of SD such as an apparent diffusion coefficient and an interface periodic distance were obtained from the Cahn theory. Phase separation occurred by nucleation and growth (NG) when paths of the composition changes were far from the critical point. SEM observation confirmed that the membrane formed by the SD mechanism had interconnected structure, whereas that by the NG mechanism had the closed cell porous structure. © 2000 John Wiley & Sons, Inc. J Appl Polym Sci 77: 776–782, 2000

Key words: phase separation; light scattering; spinodal decomposition; nucleation and growth; dry-cast process

INTRODUCTION

Porous polymeric membranes are mainly prepared by controlled phase separation of polymer solutions.[1] Phase separation of polymer solutions can be induced in two ways: nonsolvent-induced phase separation, and thermally induced phase separation (TIPS). Air casting (dry casting) of a polymer solution, precipitation from the vapor phase, and immersion precipitation are typical processes for the nonsolvent-induced phase separation.[2]

The process of nonsolvent-induced phase separation normally involves a three-component system of a polymer, a solvent, and a nonsolvent. An example of an isothermal phase diagram for a ternary component system is shown in Figure 1. Thermodynamic study, which can determine the binodal and spinodal curves, is very important to understand the membrane formation. Either nucleation and growth (NG) or spinodal decomposition (SD) can cause liquid–liquid demixing of a polymer solution. The NG mechanism occurs in the metastable region between the binodal and spinodal, whereas SD occurs in the unstable region inside the spinodal curve. Kinetic study on changes in composition due to the solvent evaporation in the dry process or due to the solvent–nonsolvent exchange in the immersion precipitation process is essential to understand and control membrane structures as well as the thermodynamics. Two examples of the composition change paths are shown in Figure 1. When the composition passes through the critical point (path 1 in Fig. 1), the phase separation occurs in the unstable region, and the structure results from the SD mechanism. On the other hand, when the composition passes slowly in the metastable region as

Correspondence to: H. Matsuyama.

Journal of Applied Polymer Science, Vol. 77, 776–782 (2000)

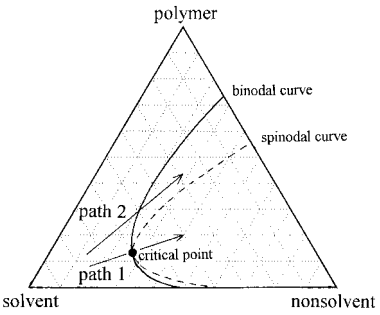

Figure 1 Example of an isothermal phase diagram for ternary component system. Solid line: binodal curve, dotted line: spinodal curve, ●: critical point.

path 2, the phase separation occurs in the NG mechanism. Studies on the type and rate of the phase separation itself are also necessary to analyze the membrane formation process.

The thermodynamics of a ternary system have been well understood in the framework of the Flory-Huggins description of polymer solutions. Altena and Smolders,[3] and Yilmaz and McHugh[4] showed numerical methods for the calculation of the binodal of liquid–liquid phase separation for polymer/solvent/nonsolvent system. Bulte et al.[5] and Cheng et al.[6] calculated the crystallization isotherm as well as the binodal envelope in the cases of crystalline polymers. Many mass transfer models have been presented in calculating the change of composition paths during the membrane formation.[7–16] Reuvers et al.[8,9] analyzed the mass transfer for a three-component system in the immersion precipitation process. Tsay and McHugh[11] presented the improved numerical model, which can predict both the solvent evaporation step and the quench step. Recently, we analyzed the mass transfer in the precipitation from the vapor phase,[16] and discussed the obtained membrane structures based on the calculated results.[17]

Contrary to these studies on thermodynamics and mass transfer, few studies were reported on kinetics of the phase separation itself in the membrane formation. Nunes and Inoue investigated the mechanism of phase separation during the immersion of cellulose acetate casting solutions in water/acetone coagulation baths.[18] They showed that the light scattering data obtained for casting solutions normally chosen for membrane preparation could be well fitted with the linear Cahn theory for spinodal decomposition. In the case of immersion of poly(ether imide) solution in a water bath, Peinemann et al.[19] studied the kinetics and mechanism of membrane formation by the light scattering.

In this work, the mechanism of phase separation during the membrane formation by the dry-cast process was investigated. Cellulose acetate was dissolved in a mixture of a relatively volatile solvent and a less volatile nonsolvent. During the evaporation of the solvent, the solubility of the polymer decreases, which induces the phase separation. Kinetics of the phase separation was studied by light scattering in addition to the clarification of the phase diagram.

EXPERIMENTAL

Materials

Polymer and solvent were cellulose acetate (CA, Aldrich Chemical Inc., acetyl content: 39.8 wt %, M_n: 30,000) and dimethylformamide (DMF, Nacalai Tesque Inc., analytical grade, b.p.: 153°C). Nonsolvent was 2-methyl-2,4-pentanediol (MPD, Nacalai Tesque Inc., analytical grade, b.p.: 197°C). Hereafter, polymer and solvent weight percent in the cast solution are abbreviated as P and S, respectively.

Cloud Point Curve

To determine the cloud curve, the polymer solutions (polymer concentration: 3, 5, 10, and 15 wt %) were prepared at 25°C. Under the constant polymer concentration, a series of solutions with the different nonsolvent concentrations were prepared. The cloud point was determined by measuring the turbidity of the solution at 500 nm wavelength by a spectrophotometer (Hitachi Co., Ltd., U-2000).

Light Scattering Measurement

The light scattering measurement was carried out with a polymer dynamics analyzer (Othuka Electronics Co., DYNA-3000). A He-Ne laser (λ = 633 nm, 5 mW) was used as a light source. Between the light source and a sample, a neutral density filter and a polarizer are set. The light scattered by the sample passes through an analyzer, and is detected by a CCD camera. The total range of angles from 0° to 40° was covered by the detector. An exposure time was 0.4 s, and the

light scattering was measured with a time interval of 9 s.

For the measurements, the polymer solution was cast on the glass plate with thickness of 25 μm. The sample was located between the laser and the detector at a room temperature of 24–26°C. The phase separation due to the evaporation of DMF was followed by a light-scattering measurement.

Membrane Morphology

The sample used for the light scattering measurement was allowed to stand for 1 day. Then the glass plate with the membrane was immersed in water, and the membrane was peeled from the plate. The dried membrane was sputtered with Au/Pd in a vacuum. The surface structure was observed by a scanning electron microscope (Hitachi Co., Ltd., S-2150) under an accelerating voltage of 15 kV.

RESULT AND DISCUSSION

According to Flory-Huggins theory,[20] Gibbs free energy of mixing for the ternary component system ΔG_m is expressed as[3]:

$$\Delta G_m/RT = n_1 \ln \phi_1 + n_2 \ln \phi_2 + n_3 \ln \phi_3 + g_{12} n_1 \phi_2 + g_{13} n_1 \phi_3 + g_{23} n_2 \phi_3 \quad (1)$$

where subscripts 1, 2, and 3 denote nonsolvent, solvent, and polymer, respectively, n_i and ϕ_i are the number of mol and the volume fraction of component i, and R and T are the gas constant and temperature. g_{ij} is the interaction parameter between component i and j. As described below, constant values were used as g_{ij} in this work. The difference between the chemical potential of component i in the mixture and in the pure state $\Delta\mu_i$ is given as follows.

$$\Delta\mu_1/RT = \ln \phi_1 + 1 - \phi_1 - (\nu_1/\nu_2)\phi_2 - (\nu_1/\nu_3)\phi_3 + (g_{12}\phi_2 + g_{13}\phi_3)(\phi_2 + \phi_3) - g_{23}(\nu_1/\nu_2)\phi_2\phi_3 \quad (2)$$

$$\Delta\mu_2/RT = \ln \phi_2 + 1 - \phi_2 - (\nu_2/\nu_1)\phi_1 - (\nu_2/\nu_3)\phi_3 + \{g_{12}(\nu_2/\nu_1)\phi_1 + g_{23}\phi_3\}(\phi_1 + \phi_3) - g_{13}(\nu_2/\nu_1)\phi_1\phi_3 \quad (3)$$

$$\Delta\mu_3/RT = \ln \phi_3 + 1 - \phi_3 - (\nu_3/\nu_1)\phi_1 - (\nu_3/\nu_2)\phi_2 + \{g_{13}(\nu_3/\nu_1)\phi_1 + g_{23}(\nu_3/\nu_2)\phi_2\}(\phi_1 + \phi_2) - g_{12}(\nu_3/\nu_1)\phi_1\phi_2 \quad (4)$$

Here, ν_i is the molar volume of component i. When an equilibrium is established between two phases, that is, a polymer-lean phase α and a polymer-rich phase β, $\Delta\mu_i$ in these two phases are equal:

$$\Delta\mu_i^\alpha = \Delta\mu_i^\beta (i = 1, 2, 3) \quad (5)$$

The liquid–liquid miscibility gap in ternary system can be calculated from eq. (5) and mass balance equations ($\Sigma\ \phi_i = 1$ for the polymer-lean phase and polymer-rich phase) and thus, the binodal can be obtained.

The equation for the spinodal is given by the following equation[3,21]:

$$G_{22}G_{33} = (G_{23})^2 \quad (6)$$

where

$$G_{ij} = \{\partial\Delta G_m/(VRT)/(\partial\phi_i\partial\phi_j)\}\nu_1 \quad (7)$$

Here, V is the total volume. The following equation are given from eq. (1).

$$G_{22} = 1/\phi_1 + (\nu_1/\nu_2)/\phi_2 - 2g_{12} \quad (8)$$

$$G_{33} = 1/\phi_1 + (\nu_1/\nu_3)/\phi_3 - 2g_{13} \quad (9)$$

$$G_{23} = 1/\phi_1 - g_{12} - g_{13} + (\nu_1/\nu_2)/g_{23} \quad (10)$$

The spinodal can be calculated from eq. (6) and the mass balance equation.

To obtain the binodal and spinodal, several parameters must be determined. The values of ν_1, ν_2, and ν_3 used for the calculation were 128, 76.9, and 23080, respectively. The nonsolvent–polymer interaction parameter g_{13} determined from the swelling experiment was reported as 1.11[22] for MPD/CA system. The solvent–polymer interaction parameter g_{23} can be roughly estimated from eq. (11) by the solubility parameter δ.[23]

$$g_{23} = 0.35 + \nu_2/(RT)(\delta_2 - \delta_3)^2 \quad (11)$$

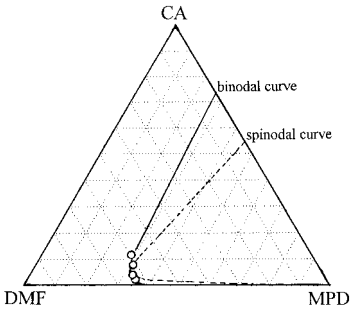

Figure 2 Phase diagram for CA/DMF/MPD. Solid line: binodal curve, dotted line: spinodal curve, ○: experimental data of cloud point.

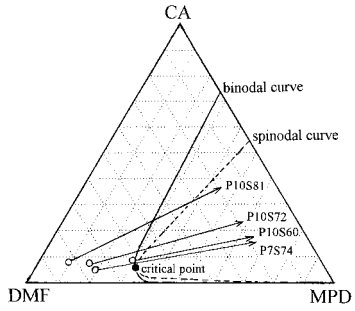

Figure 3 Paths of the composition change in the membrane formation. Solid line: binodal curve, dotted line: spinodal curve, ●: critical point, ○: initial composition.

The solubility parameters of CA and DMF were reported as 25.1 $MPa^{1/2}$ [24] and 24.8 $MPa^{1/2}$,[25] respectively. The value of g_{23} was estimated as 0.352. g_{12} was a fitting parameter.

The calculated binodal and spinodal curves are shown in Figure 2 as solid and dotted lines, respectively, when 0.3 was used as g_{12}. The binodal is in accordance with circles (○) in Figure 2, which are the experimental data for the cloud point.

To estimate the composition paths during the membrane formation, mathematical models have been developed.[7–16] Their sophisticated models, however, are difficult to use because of the complicated numerical procedures for solving the simultaneous partial differential equations. Therefore, we obtained the composition paths by assuming that only DMF evaporate as the first approximation because the boiling point of DMF (153°C) is much lower than that of MPD (197°C). Under this assumption, the composition will change on the straight line connecting a point of initial composition to a point of pure solvent. Initial compositions in the cast solutions used in this work were P10S60, P10S72, P10S81, and P7S74. The paths of the composition change in the respective cases are shown in Figure 3, based on our rough assumption. Further study on the mass transfer is necessary to obtain the accurate paths.

An example of the relation between the scattered light intensity I_s and the scattered angle θ in the case of P10S72 is shown in Figure 4. Clear maxima of the intensity were recognized at the scattered angle of about 9°. As time proceeds, the position of the maximum was almost unchanged, while the scattered intensity increased. This result clearly shows that the phase-separation mechanism in this time scale is in the early stage of spinodal decomposition. Similar maxima in I_s were observed in the cases of P10S72 and P7S74.

According to the linear Cahn theory[26] in the early stage of SD, I_s can be related with time t in the following equation.

$$I_s(q, t) \propto \exp\{2R(q)t\} \tag{12}$$

Here, $R(q)$ is a growth rate of the concentration fluctuation. Wave number q is expressed as:

$$q = (4\pi n/\lambda_0)\sin(\theta/2) \tag{13}$$

where n is the solution refractive index, and λ is the wavelength *in vacuo*. The wave number of maximum scattered light intensity q_m can be correlated to the average interphase distance Λ_m in eq. (14).

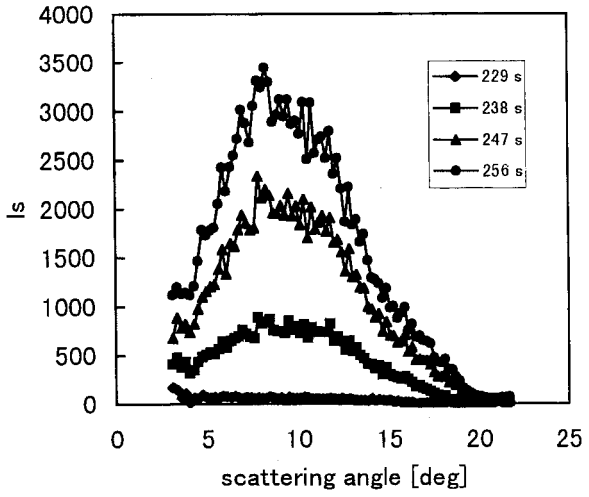

Figure 4 Relation between the scattered light intensity and the scattered angle in the case of P10S72.

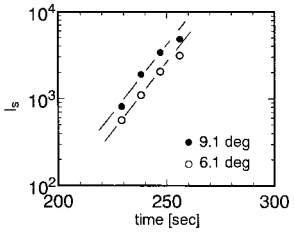

Figure 5 Semi-logarithmic plots of I_s against time for the data in Figure 4.

$$q_m = 2\pi/\Lambda_m \tag{14}$$

$R(q)$ is given by[27,28]:

$$R(q) = D_{\text{app}}q^2\{1 - q^2/(2q_m^2)\} \tag{15}$$

where D_{app} is the apparent diffusion coefficient. Thus, we can expect that the plot of $R(q)/q^2$ vs. q^2 is linear in the early stage of SD. The intercept of the linear line gives D_{app}. q_m can be determined from the slope of the linear line in addition to from the direct measurement of I_s versus θ.

Semilogarithmic plots of I_s against time for the data in Figure 4 are shown in Figure 5. As expected from eq. (12), the linear relations were obtained. Figure 6 shows plots of $R(q)/q^2$ as a function of q^2 in the cases of P10S60, P10S72, and P7S74. In all cases, linear relations were recognized, which is in accordance with the expectation from eq. (15). As shown in Figure 3, the composition change paths in these three cases are relatively close to the critical point. This is the reason for the SD mechanism rather than the NG mechanism.

Characteristic properties of phase separation in the early stage of SD, which were obtained from the plots in Figure 6, are summarized in Table I. The values of D_{app} decreased in the order of P7S74, P10S60, and P10S72 cases. In the con-

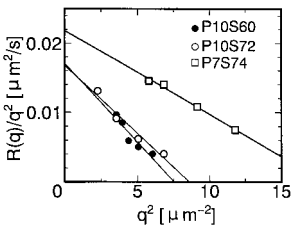

Figure 6 Relation between $R(q)/q^2$ and q^2.

Table I Characteristic Properties of Phase Separation in the Early Stage of SD

System	D_{app} [μm^2/s]	q_m [μm^{-1}]^a	q_m [μm^{-1}]^b	Λ_m [μm]
P10S60	1.70×10^{-2}	2.97	1.92	2.1
P10S72	1.67×10^{-2}	2.23	2.12	2.8
P7S74	2.19×10^{-2}	3.22	3.02	2.0

[a] Determined from the light scattering data.
[b] Obtained from the linear relations shown in Figure 6.

tent of mean-field approximation, D_{app} in the early stage of SD is given by[27,29]:

$$D_{\text{app}} = D_c(\chi - \chi_s)/\chi_s \tag{16}$$

where D_c is the translational diffusion coefficient of molecules, and χ and χ_s are the Flory-Huggins interaction parameters at the condition where phase separation occurs and on spinodal curve, respectively. Thus, D_{app} is influenced by both kinetic property (D_c) and thermodynamic property [$(\chi - \chi_s)/\chi_s$). When D_c is high due to, for example, the low viscosity of the solution, D_{app} becomes high. The higher quench depth leads to the increase of $(\chi - \chi_s)/\chi_s$, which results in the higher D_{app}. As shown in Figure 3, the polymer concentrations at which the composition change paths cross the binodals increase in the order of P7S74, P10S60, and P10S72 cases. Because the increase of the polymer concentration in the solution brings about the increase of the viscosity, this may be the reason for the decrease of D_{app} in this order. The interphase periodic distance Λ_m ranged from 2 to 3 μm. Further, q_m directly determined from the light scattering shown in Figure 4 is roughly in agreement with those obtained from the linear relations shown in Figure 6.

The relation between I_s and θ in the case of P10S81 is shown in Figure 7. In contrast to Figure 4, no maximum in I_s was observed in this case. Thus, the promising phase-separation mechanism is not by SD, but NG. Hashimoto et al.[30] reported that in the NG mechanism of phase separation of a polymer blend system, the scattered intensity monotonously decreased with θ, and the intensity level itself increased with time. Our result shown in Figure 7 agrees with this observation.

In the NG mechanism, I_s at a fixed angle θ, is related with time t to a power law[18,31]:

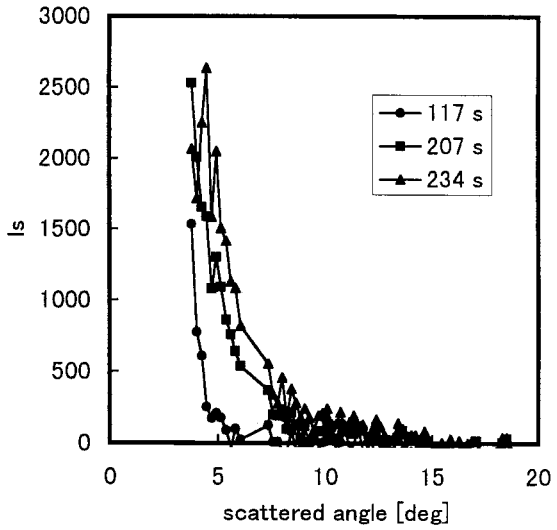

Figure 7 Relation between the scattered light intensity and the scattered angle in the case of P10S81.

$$I_s \propto (t - \tau)^n \tag{17}$$

where τ is the time when nucleation starts. Homogeneous nucleation gives 4.0 for n, whereas heterogeneous nucleation gives 3.0. Logarithmic plot of I_s against $(t - \tau)$ for the data of Figure 7 are shown in Figure 8. Here, the time when I_s starts to increase was used as τ. As can be seen in Figure 8, linear relations were obtained, which is in agreement with the expectation from eq. (17). The slope values were about 4.0. The homogeneous nucleation may occur in this condition. Nunes and Inoue also reported the slope values of about 4.0 in the NG mechanism in CA/acetone/water system.[18] As shown in Figure 3, the composition change path in P10S81 system is far from the critical point, which is in contrast to the other three cases. Thus, the composition passes in the metastable region for longer time and the phase separation is likely to occur in this region rather than in the unstable region. This is the reason for the phase separation in the NG mechanism in the P10S81 case.

Figure 9 shows membrane surface structures. In the P10S60, P10S72, and P7S74 cases, the SD mechanism was confirmed for the phase separation by the light-scattering experiment, while the NG mechanism was confirmed in the P10S81 case. Interconnected structures can be observed in the P10S60, P10S72, and P7S74 cases, which coincides with the structure expected from the SD mechanism. There is no distinguished difference in these three structures. The interphase periodic distance in Figure 9(a), (b), and (c), which corresponds to a length from a pore center to another pore center is about 1 μm. This value is lower than Λ_m in the early stage of SD shown in Table I. This may be attributable to membrane shrinkage by the evaporation of DMF or by the immersion in water after the dry process. Further study is necessary to clarify the difference in these periodic distances. Figure 9(d) shows isolated spherical pores in P10S81 case. This is the typical structure expected from the NG mechanism.

CONCLUSION

1. The cloud points in the CA/DMF/MPD system were measured, and the binodal and the spinodal curves were calculated based on the Flory-Huggins theory. The approximate paths of composition changes due to the evaporation of DMF were presented in the phase diagram.
2. It was found by the light scattering experiment that the phase separation occurred by the spinodal decomposition (SD) mechanism when the composition change paths were close to the critical point. Characteristic properties of the early stage of SD such as D_{app}, q_m, and Λ_m were obtained according to the Cahn theory. D_{app} decreased as the polymer concentration at which phase separation occurs increased. On the contrary, the light-scattering experiment revealed that the phase separation obeyed the nucleation and growth (NG) mechanism when the composition change path was far from the critical point.
3. The resultant membrane morphology was observed by SEM. It was confirmed that the structure formed by the SD mechanism

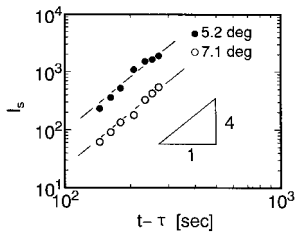

Figure 8 Logarithmic plots of I_s against $t - \tau$ for the data in Figure 7.

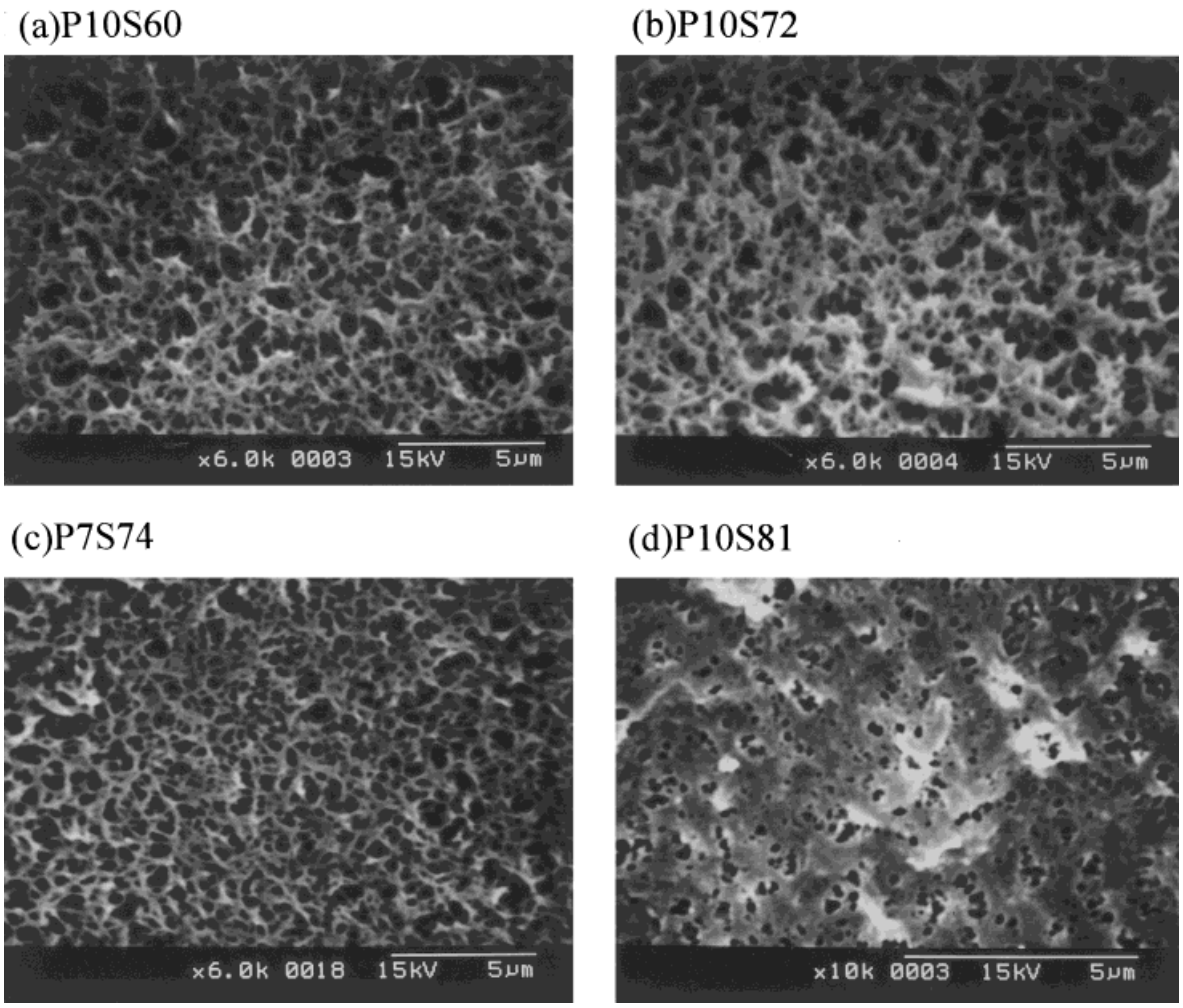

Figure 9 Membrane surface structures for various cases.

had interconnected pores, whereas the structure by the NG mechanism had isolated spherical pores.

REFERENCES

1. Mulder, M. Basic Principles of Membrane Technology; Kluwer Academic Publishers: Dordrecht, 1996, p. 74.
2. van de Witte, P.; Dijkstra, P. J.; van den Berg, J. W. A.; Feijen, J. J Membr Sci 1996, 117, 1.
3. Altena, F. W.; Smolders, C. A. Macromolecules 1982, 15, 1491.
4. Yilmaz, L.; McHugh, A. J. J Appl Polym Sci 1986, 31, 997.
5. Bulte, A. M. W.; Naafs, E. M.; van Eeten, F.; Mulder, M. H. V.; Smolders, C. A.; Strathmann, H. Polymer 1996, 37, 1647.
6. Cheng, L. P.; Dwan, A. H.; Gryte, C. C. J Polym Sci Polym Phys 1994, 32, 1183.
7. Cohen, C.; Tanny, G. B.; Prager, S. J Polym Sci Polym Phys 1979, 17, 477.
8. Reuvers, A. J.; van den Berg, J. W. A.; Smolders, C. A. J Membr Sci 1987, 34, 45.
9. Reuvers, A. J.; Smolders, C. A. J Membr Sci 1987, 34, 67.
10. Tsay, C. S.; McHugh, A. J. J Polym Sci Polym Phys 1990, 28, 1327.
11. Tsay, C. S.; McHugh, A. J. J Polym Sci Polym Phys 1991, 29, 1261.
12. Radovanovics, P.; Thiel, S. W.; Hwang, S. T. J Membr Sci 1992, 65, 213.
13. Cheng, L. P.; Soh, Y. S.; Dwan, A.; Gryte, C. C. J Polym Sci Polym Phys 1994, 32, 1413.
14. Shojaie, S. S.; Krantz, W. B.; Greenberg, A. R. J Membr Sci 1994, 94, 255.

15. Shojaie, S. S.; Krantz, W. B.; Greenberg, A. R. J Membr Sci 1994, 94, 281.
16. Matsuyama, H.; Teramoto, M.; Nakatani, R.; Maki, T. J Appl Polym Sci, submitted.
17. Matsuyama, H.; Teramoto, M.; Nakatani, R.; Maki, T. J Appl Polym Sci, submitted.
18. Nunes, S. P.; Inoue, T. J Membr Sci 1996, 111, 93.
19. Peinemann, K. V.; Maggioni, J. F.; Nunes, S. P. Polymer 1998, 39, 3411.
20. Flory, P. J. Principles of Polymer Chemistry; Cornell University Press: Ithaca, NY, 1953.
21. Tompa, H. Polymer Solutions; Butterworths: London, 1956.
22. Matsuyama, H.; Teramoto, M.; Uesaka, T. J Membr Sci 1997, 135, 271.
23. Bristow, G. M.; Watson, W. F. Trans Farad Soc 1958, 54, 1731.
24. Barton, A. F. M. Handbook of Polymer–Liquid Interaction Parameter; CRC Press: Boca Raton, FL, 1990.
25. Barton, A. F. M. Handbook of Solubility Parameters and Other Cohesion Parameter; CRC Press: Boca Raton, FL, 1991.
26. Cahn, J. W. J Chem Phys 1965, 42, 93.
27. Hashimoto, T.; Kumaki, J.; Kawai, H. Macromolecules 1983, 16, 641.
28. Lal, J.; Bansil, R. Macromolecules 1991, 24, 290.
29. Sasaki, K.; Hashimoto, T. Macromolecules 1984, 17, 2818.
30. Hashimoto, T.; Sasaki, K.; Kawai, H. Macromolecules 1984, 17, 2812.
31. Boom, R. Membrane Formation by Immersion Precipitation: The Role of a Polymeric Additive; PhD Thesis, University of Twente (1992).